Propagation From Geostationary Orbit Satellite to Ground Station Considering Dispersive and Inhomogeneous Atmospheric Environments

CHANGSEONG KIM[1], (Student Member, IEEE), JUN HEO[1], (Student Member, IEEE), KYUNG-YOUNG JUNG[2], (Senior Member, IEEE), HOSUNG CHOO[3], (Senior Member, IEEE), AND YONG BAE PARK[1, 4], (Senior Member, IEEE)

[1]Department of AI Convergence Network, Ajou University, Gyeonggi-do 16499, South Korea
[2]Department of Electronic Engineering, Hanyang University, Seoul 04763, South Korea
[3]School of Electronic and Electrical Engineering, Hongik University, Seoul 04066, South Korea
[4]Department of Electrical and Computer Engineering, Ajou University, Gyeonggi-do 16499, South Korea

Corresponding author: Yong Bae Park (yong@ajou.ac.kr)

ABSTRACT We propose a novel method to calculate the propagation from a geostationary orbit (GEO) satellite to a ground station considering dispersive and inhomogeneous atmospheric environments with an actual satellite parabolic reflector antenna. The proposed simulation method is based on the hybrid numerical techniques including physical optics (PO), the 3-dimensional (3-D) ray tracing technique, and geometrical optics (GO). The electromagnetic propagation from an actual GEO satellite parabolic reflector antenna to a ground station at Seoul, Korea is calculated using PO. Reflections and refractions at the boundaries of the stratified refractive index model for the atmosphere are then calculated by the ray tracing approach and GO to take into account inhomogeneous atmospheric environments. Our method is verified by comparing with the results with the prediction method of rain attenuation given in ITU-R P.618-13 and the unified model. The comparison generally shows a good agreement. Atmospheric attenuation and boresight errors from a GEO satellite to a ground station are calculated and discussed. As a result of the calculations, when the rainfall rate is 26.19 mm/h, the atmospheric attenuation from a GEO satellite (COMS-1) to a ground station at Seoul, Korea is 12.1621 dB and the boresight error is 0.0336 degrees.

INDEX TERMS Atmospheric environments, 3-D ray tracing technique, geometrical optics, physical optics, dispersive and inhomogeneous media.

I. INTRODUCTION

To estimate the characteristics of geostationary orbit (GEO) satellite links for navigation, communications, broadcasting and surveillance, it is necessary to accurately calculate the electromagnetic wave propagation in the atmosphere. In general, the atmospheric environment affects the attenuation and refraction of electromagnetic wave propagation on satellite links [1]–[4]. Electromagnetic waves are reflected, refracted and absorbed when they pass through the atmosphere. The atmosphere can be classified into five layers according to altitude: the troposphere, the stratosphere, the mesosphere,

the thermosphere, and the exosphere with their altitudes ranging from 0 to about 10000 km. In the troposphere and stratosphere, below 30 km, the atmospheric effects depend on the temperature, air pressure, relative humidity, and suspended droplets [5], [6]. In the ionosphere, which includes the thermosphere, parts of the mesosphere, and exosphere between 60-1000 km, atmospheric effects depend on the ionized particles. The region from the upper stratosphere to the boundary of the ionosphere is approximated with vacuum due to low temperature and low integrated water vapor [7], [8]. In addition, the atmosphere above 1000 km is also approximated with vacuum due to the low density of gases. Thus, electromagnetic wave propagation is mainly affected by the troposphere and ionosphere, where the critical effects on

The associate editor coordinating the review of this manuscript and approving it for publication was Santi C. Pavone.

electromagnetic wave propagation are attributed to oxygen, water-vapor molecules, and free electrons.

The atmospheric environments have been monitored using radiosonde, ionosonde, magnetometer, and solar flux monitor [9], [10]. In addition, atmospheric absorption and rain attenuation have also been measured or calculated to estimate the influence of the troposphere and ionosphere on the wave propagation [11]–[17]. Atmospheric attenuation of electromagnetic waves was measured at 58, 94, and 122 GHz by the Czech metrology institute, while at 19.7 GHz by Universidad Politécnica de Madrid using the Eutelsat Hot Bird 13A Ka-band beacon [11], [12]. Studies have been conducted on predictive models for calculating atmospheric absorption and refraction [13], [14]. Rain attenuation was calculated using probability of rainfall rate and radiometric measurements [15]–[17].

However, the theoretical analysis of electromagnetic wave propagation considering dispersive and inhomogeneous atmospheric environments seems to be lacking. It is very difficult to apply the numerical techniques such as the finite-difference time-domain (FDTD) method, finite element method (FEM), and methods of moments (MOM) into the actual atmosphere, because they require huge computational resources. Some models which analyze the electromagnetic wave propagation in dispersive media have been studied using the FDTD method, but have not been applied to the actual atmosphere [18], [19]. In addition, the parabolic equation can be used to analyze wave propagation in the atmosphere to reduce computational resources, but it has limitation that the result is accurate only in a limited angular range from the antenna beam [20].

The method given in ITU-R P.676-12 to calculate the atmospheric gaseous attenuation has been suggested considering air pressure, temperature, and humidity as a summation of the individual spectral lines from oxygen and water vapor [16]. However, this method uses only a line-by-line summation of gaseous attenuation without considering atmospheric reflections. Also, the rain attenuation model is suggested by ITU-R P.618-13 and Mello and Pontes [4], [21]. But these models did not include the boresight error and phase dispersion, and the only rainfall attenuation was calculated. In the previous study, we analyzed electromagnetic wave propagation in the atmosphere using the 2-dimensional ray-tracing technique [22]. However, we did not apply to the 3-dimensional (3-D) space, did not compare our results with measured data, and did not accurately consider the dispersive refractive index of the atmosphere. Moreover, the study on the electromagnetic wave propagation from the actual antennas of GEO satellites to a ground station seems to be insufficient. Therefore, it is necessary to accurately compute the atmospheric attenuation, boresight error, and phase dispersion, taking into account dispersive and inhomogeneous atmospheric environments. Herein, the radiation from an actual GEO satellite antenna should be considered for more accurate prediction of wave propagation in the satellite links.
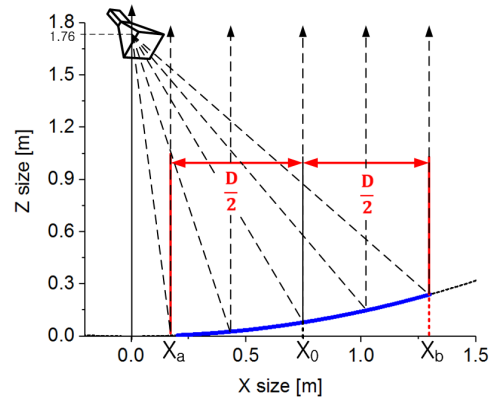

FIGURE 1. Offset parabolic reflector antenna configuration used in calculation (D = 1.1 m, Xa = 0.2 m, X0 = 0.75 m, Xb = 1.3 m F = 1.76 m, Gain = 41.36 dBi, and 3dB Beamwidth = 1.84°).

In this paper, we propose a novel method to calculate the propagation from a GEO satellite to a ground station considering dispersive and inhomogeneous atmospheric environments with an actual satellite parabolic antenna. The proposed simulation method is based on hybrid numerical techniques including physical optics (PO), the 3-D ray tracing technique, and geometrical optics (GO). The equivalent surface currents of reflector meshes are calculated using PO. Reflections and refractions at the boundaries of the stratified refractive index model for the atmosphere are calculated using 3-D ray tracing technique and GO. The effective refractive index is calculated from electron density of the ionosphere and meteorological conditions of the troposphere. Our method is verified by comparing with the results with the prediction method of rain attenuation given in ITU-R P.618-13 and the unified model [4], [21]. Atmospheric attenuation and boresight errors from GEO satellites to a ground station at Seoul, Korea are calculated using the proposed hybrid method, and the results are discussed in detail.

II. ANALYSIS PROCEDURE

A. RADIATION FROM OFFSET PARABOLIC REFLECTOR ANTENNA

The offset parabolic antenna configuration used in this work is shown in Fig. 1. The reflector size and focal length are the same as the reflector antenna specifications of communication, ocean and meteorological satellite-1 (COMS-1), and the material of the reflector is assumed to be a perfect electrical conductor [23]. The feed antenna of the parabolic reflector is a pyramidal horn with a 10-dB beamwidth of 29.13 degrees. The surface of the parabolic reflector is divided into meshes, and the distance between two centers of adjacent meshes is less than 1/10 wavelength [24]. The equivalent surface current density is calculated using PO. The electromagnetic field of the horn antenna is calculated in [25], and the radiated electromagnetic fields are calculated as the product of surface area and the surface current density.

B. ATMOSPHERIC ENVIRONMENTS

To consider the refraction, reflection, and absorption in atmospheric environments, we use the effective complex

TABLE 1. Refractivity Of Ionospheric Layers (I-Cheon, South Korea, Aug. 14, 2019, 12:00).

	f_p	N			
	[MHz]	1 GHz	10 GHz	20 GHz	30 GHz
E-layer (110 km)	0.35	-0.0613	-6.13E-4	-1.53E-4	-6.81E-5
F-layer (289.7 km)	5.250	-13.78	-0.1378	-0.0345	-0.0153

refractive index of the atmosphere, which is determined by the frequency, air pressure, air temperature, water-vapor pressure, electron density, and magnetic field of earth. The atmosphere is stratified by altitude, and the effective complex refractive index n of each layer is calculated from the complex refractivity N using (1). The complex refractivity of the troposphere and stratosphere is the central quantity computed by the millimeter-wave propagation model (MPM) [5], [6]. The propagation constant γ and intrinsic impedance η are calculated by using refractive index n, permeability of vacuum μ_0, permittivity of vacuum ε_0, angular frequency ω in (2), (3). The relative permeability of the atmosphere is assumed to be 1.

$$n = 1 + N \times 10^{-6} = 1 + (N' - jN'') \times 10^{-6} \quad (1)$$

$$\gamma = j\beta + \alpha = j\omega\sqrt{\mu_0\varepsilon_0}(n' - jn'') \quad (2)$$

$$\eta = \sqrt{\frac{j\omega\mu}{j\omega\varepsilon + \sigma}} = \eta_0\frac{1}{n' - jn''} \quad (3)$$

In the ionosphere, free electrons exist for a short period before they are captured by positive ions and affect electromagnetic wave propagation. Our target frequency is above 1 GHz, it is permissible to neglect electron collisions and magnetic field of earth [26]. The effective refractive index of the ionosphere is calculated by the simplified Appleton Hartree equation (4) [27].

$$n^2 = 1 - (\frac{\omega_p}{\omega_0})^2 \quad (4)$$

$$P_{fluc} = 27.5S_4^{1.26} \quad (5)$$

In (4), ω_p is plasma frequency which is calculated from electron density in the ionosphere. Ionosonde data including plasma frequency is provided by DIDBASE [28]. Ionospheric attenuation includes the ionospheric absorption and ionospheric scintillation, which reduces the amplitude of the received signal. The ionospheric absorption is cited in ITU-R P.531-14, and peak-to-peak fluctuations P_{fluc} of the ionospheric scintillation is calculated by (5) [29]. S_4 is the scintillation index and can be provided by [30]. The real refractivity of the ionosphere has a negative value and is shown in Table 1. As the frequency increases, ionospheric effects decrease, and above 10 GHz, ionospheric effects can be negligible.

The real and imaginary refractivity in air by frequency is shown in Fig. 2 and Fig. 3. The refractivity N is calculated from air pressure, air temperature, and relative humidity. Dispersion of the complex refractivity represents the
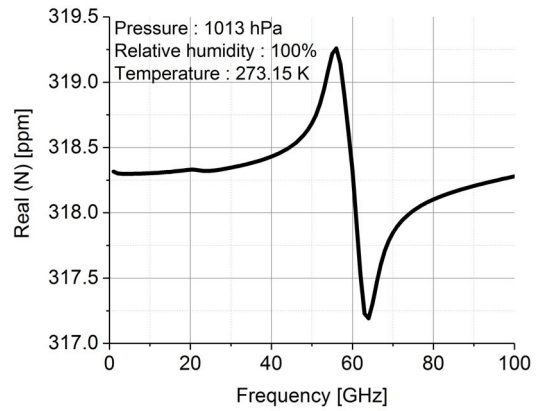

FIGURE 2. Real refractivity in parts per million of saturated air (relative humidity: 100%) at sea level for temperature T = 273.15 K below 100 GHz.
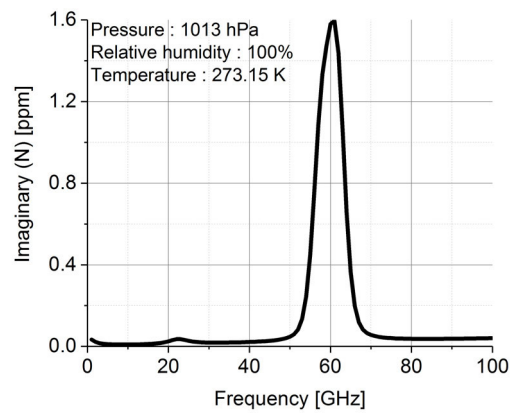

FIGURE 3. Imaginary refractivity in parts per million of saturated air (relative humidity: 100%) at sea level for temperature T = 273.15 K below 100 GHz.
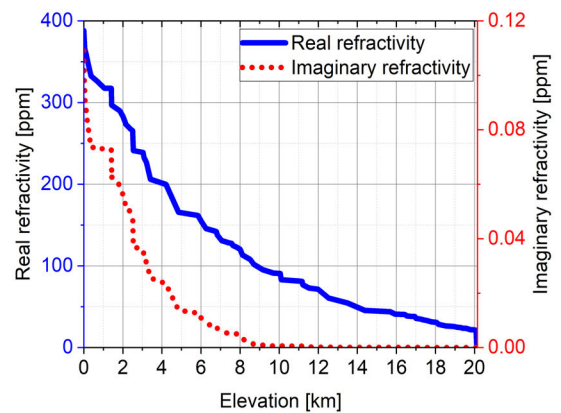

FIGURE 4. Refractivity in atmospheric environments (30 GHz, Osan, Korea, Aug. 14, 2019).

resonance contribution of absorber molecules of water vapor and oxygen.

Fig. 4 shows the refractivity of the Osan's atmosphere in South Korea calculated from meteorological data [31]. As the elevation increases, the air density decreases and the effective refractivity approaches zero. The imaginary refractivity has
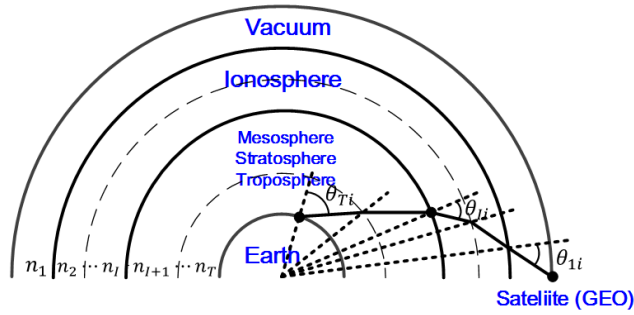
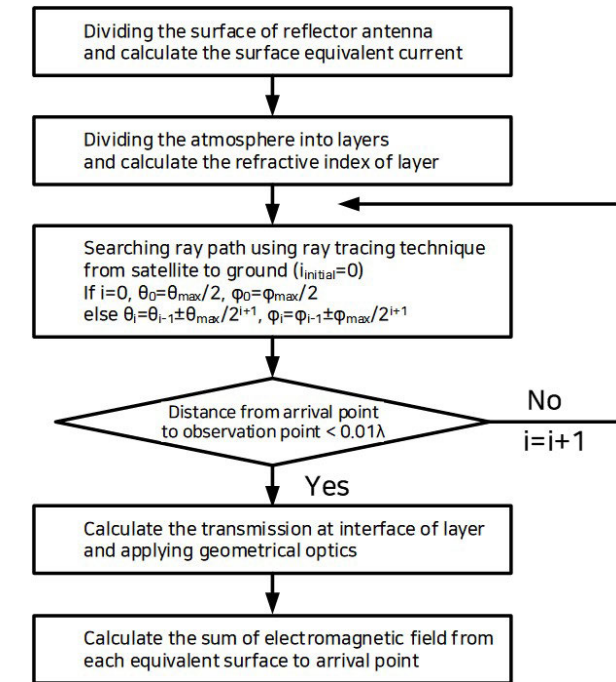**FIGURE 5.** Problem geometry of the ray tracing technique in atmosphere.

FIGURE 6. Overall analysis procedure for electromagnetic wave propagation.

FIGURE 7. Reflection and transmission at an oblique angle upon a dielectric-dielectric interface.

a large value in the vicinity of the resonant frequency of the gas.

Fig. 5 and Fig. 6 show the problem geometry and overall analysis procedure for electromagnetic wave propagation. The electromagnetic wave propagation is approximated in the atmosphere using high-frequency approximation techniques such as PO, 3-D ray tracing, and GO.

We divide the surface of the reflector antenna into meshes and calculate the equivalent surface current of each mesh using PO. The distance between two centers of adjacent meshes is less than 1/10 wavelength for accuracy of results.

Note that we divide the atmosphere by elevation, and the effective complex refractive index of stratified layers is calculated from meteorological data such as humidity, air temperature, and air pressure. Then, we can search the ray path considering the reflection and the refraction at the layers using the 3-D ray tracing technique. The ray path is updated until the distance between the actual arrival point and the observation point is less than hundredth of wavelength.
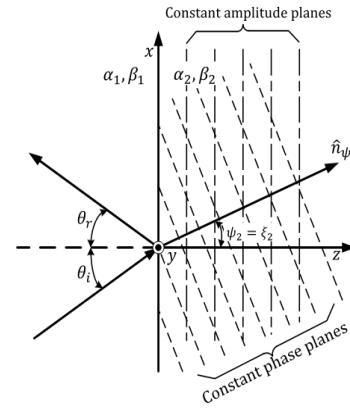
Increasing the number of iterations by 1 makes both the zenith angle θ and azimuth angle ϕ accurate, and the maximum error is halved. If this condition is satisfied, the ray path is fixed and the electromagnetic fields can be calculated from the equivalent surface currents of the reflector and geometrical optics. When the electromagnetic waves encounter the boundary of stratified lossy layers, the electromagnetic fields are calculated by using (6)-(10). Note that the equation (10) is given by geometrical optics.

Fig. 7 shows the reflection and transmission at an oblique angle upon a dielectric-dielectric interface. We resolve an arbitrarily polarized incident wave into components that are parallel field $E_{||}$ and perpendicular field $E_{\perp}$ to the plane of incidence, and calculate the reflection and transmission coefficients of each component $T_{||}$ and $T_{\perp}$. The refractive angle θ_t is the complex value and is not the true refractive angle of ray path. The true refractive angle ψ_2 is calculated if the propagation constant of the media α and β is obtained in (9). In (10), ρ_0 is the distance from source to current layer and s is the distance from current layer to the next layer.

$$E^t(x, z) = (T_{\perp}E^i_{\perp} + T_{||}E^i_{||})e^{-(zp+\alpha_1 x \sin\theta_i)}e^{-(zq+\beta_1 x \sin\theta_i)}$$

$$(6)$$

$$p = |\cos\theta_t| \{\alpha_2 \cos[\arctan(\frac{\text{Im}(\cos\theta_t)}{\text{Re}(\cos\theta_t)})]$$

$$- \beta_2 \sin[\arctan(\frac{\text{Im}(\cos\theta_t)}{\text{Re}(\cos\theta_t)})]\}$$

$$(7)$$

$$q = |\cos\theta_t| \{\alpha_2 \sin[\arctan(\frac{\text{Im}(\cos\theta_t)}{\text{Re}(\cos\theta_t)})]$$

$$+ \beta_2 \cos[\arctan(\frac{\text{Im}(\cos\theta_t)}{\text{Re}(\cos\theta_t)})]\}$$

$$(8)$$

$$\psi_2 = \tan(\frac{\beta_1 \sin\theta_1}{q})$$

$$(9)$$

$$E^i_n = E^t_{(n-1)}\frac{\rho_0}{\rho_0 + s}e^{-(zp+\alpha_1 x \sin\theta_i)}e^{-(zq+\beta_1 x \sin\theta_i)} \quad (10)$$

The direction of transmission wave is calculated using the 3-D ray tracing technique. The transmission angle at the boundary is calculated by (9). After the direction of the transmission angle and transmitted field are

TABLE 2. Comparison of atmospheric effects calculated by our method and ITU-R P.676-12 model (Osan, South Korea, Aug. 14, 2019, 12:00, 20 GHz).

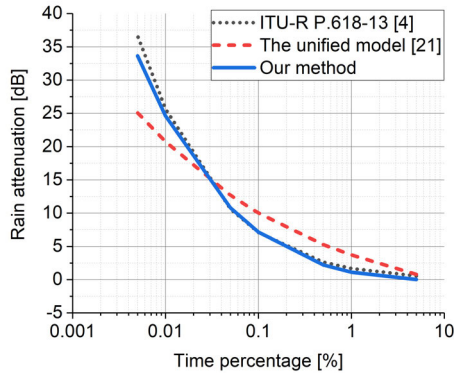| Atmospheric effects	Power attenuation [dB]	Phase dispersion [degrees]	Boresight error [degrees]
ITU-R P.676-12 [16]	1.1368	-7.2474	-
Our method (point source)	1.3396	-7.2682	4.98×10^{-6}

FIGURE 8. Comparison of rain attenuation calculated by our method, ITU-R P.618-13, and the unified model (20 GHz, Tx: GEO satellite (COMS-1), Rx: South Korea, rain height: 3.601 km [37]).

determined, the transmitted wave is defined by the incident wave at the next boundary of the layer. Once the transmitted wave of the boundary is obtained, we can calculate the incident wave at the next boundary using the GO approximation by (10) [32]. This computation is iterated until arriving the final atmospheric layer. When the electromagnetic field is obtained at the observation point, we can calculate atmospheric attenuation and refraction.

C. NUMERICAL RESULTS

We calculate the atmospheric attenuation and refraction of electromagnetic wave using PO, 3-D ray tracing technique, and GO. Atmospheric attenuation consists of (1) the reflection at boundary of stratified layers due to change of the refractive index, (2) the attenuation within the stratified layer calculated from the imaginary part of refractive index, and (3) the ionospheric attenuation. The ionospheric attenuation is calculated by considering scintillation coefficient at target frequency and ionospheric absorption.

Table 2 shows the comparison of atmospheric effects by calculated by our method and ITU-R P.676-12. The ITU-R P.676-12 provides attenuation by atmospheric gases and related effects, excluding boresight error. But our method can calculate the boresight error through the electromagnetic field analysis using the hybrid numerical techniques including physical optics (PO), the 3-dimensional (3-D) ray tracing technique, and geometrical optics (GO).

To check the accuracy of our method, the rain attenuation is calculated and compared with the prediction method of ITU-R P. 618-13 and the unified model at 20 GHz, which provides the rain attenuation versus time percentage, as shown in Fig. 8 [4], [21]. A short duration precipitation rate is needed
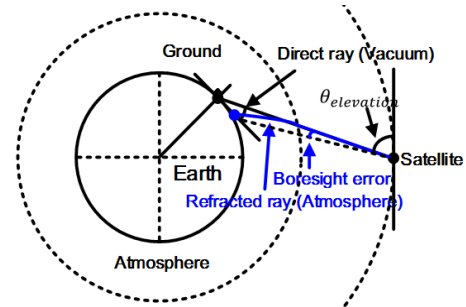

FIGURE 9. Problem geometry for calculation of boresight error on downlink.

to assess the rainfall attenuation [33], [34]. To account for the atmospheric environment, it is more accurate to use a short-term precipitation than a long-term precipitation. The International Telecommunication Union (ITU) has implicitly accepted a 1-minute integration time as the most desirable for rain attenuation prediction [34]. Therefore, our method uses short duration precipitations including the 1-minute rainfall rate. Time percentage is defined as a cumulative distribution of descending data. For example, if time percentage is 0.1% and rain attenuation is 9.52 dB, the rain attenuation exceeds 9.52 dB for 0.1% of the total time. In order to compare our results with ITU-R data, we obtained the rainfall rate corresponding to time percentage [35], [36]. The time percentages of 5, 1, 0.5, 0.1, 0.05, 0.01, and 0.005% correspond to the rainfall rates 0.157, 3.46, 6.33, 18.14, 26.19, 54.8, and 72.5 mm/h, respectively. This rainfall rate is calculated as a part of the effective refractive index N by the MPM [5], [6] in our calculation. Also, we use a fixed rainfall cloud height and assume that the rainfall cloud height is 3.601 km [37]. And the number of layers of the atmosphere is 81.

The boresight error is an angle difference between the direct ray in vacuum and the actual ray in atmospheric environments. Fig. 9 shows a problem geometry for calculation of the boresight error. We can determine the number of stratified layers of the atmosphere for accurate calculations through convergence of boresight error.

As the atmospheric refraction increases, the boresight error increases. Convergence of the boresight error is shown in Fig. 10. The number of layers indicates the number of stratified layers in the troposphere and stratosphere. The converged boresight errors are 0.0000048 degrees for the downlink. The boresight error converges if the atmosphere is stratified into 50 or more layers. Note that 80 layers in Fig. 10 is enough for convergence and the number of layers used in Figs 11 through 14 is 80.

Fig. 11 shows the atmospheric attenuation in the troposphere, stratosphere, and ionosphere. The meteorological data were measured at Osan in South Korea. Atmospheric effects include the effects of the troposphere, stratosphere, and ionosphere on the attenuation. Tropospheric and stratospheric effects are calculated assuming that the ionosphere is a vacuum. Also, Ionospheric effects are computed assuming that the troposphere and stratosphere are vacuum. We used the gigahertz scintillation model given in ITU-R P. 531-13 to
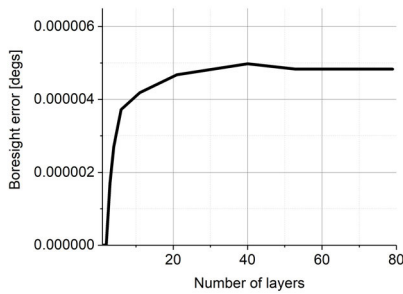
FIGURE 10. Convergence of boresight error on downlink (20 GHz, earth station: 37.546°N, 126.883°E, satellite: GEO, 128.2°E (COMS-1)).
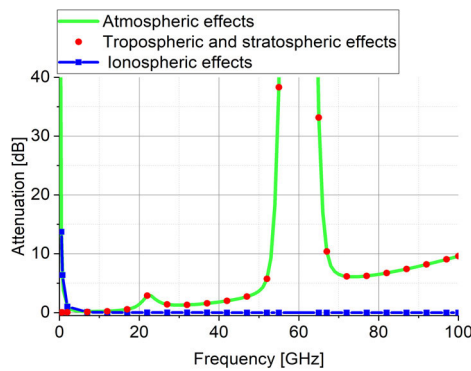

FIGURE 11. Atmospheric attenuation on downlink according to frequency (earth station: 37.546°N, 126.883°E, satellite: GEO, 128.2°E (COMS-1), Osan, South Korea, Aug. 14, 2019).
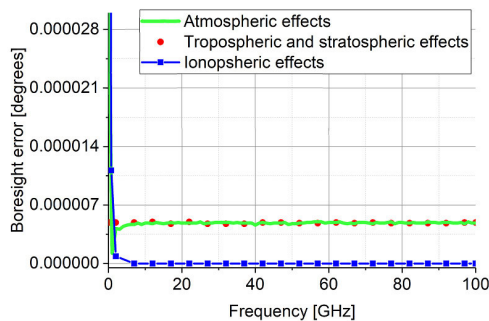

FIGURE 12. Boresight error on downlink according to frequency (earth station: 37.546°N, 126.883°E, satellite: GEO, 128.2°E (COMS-1), Osan, South Korea, Aug. 14, 2019).

calculate the ionospheric attenuation assuming that the peak-to-peak amplitude fluctuation of the ionospheric scintillation is 1 dB at 2 GHz [28]. At 5 GHz or less, ionospheric attenuation is dominant, but it decreases rapidly as the frequency increases. Attenuations in the troposphere and stratosphere have large values at around the resonant frequency of oxygen (22.3 GHz) and water-vapor (60 GHz) molecule.

Fig. 12 shows the boresight error in the troposphere and ionosphere. Atmospheric effects include the effects of the troposphere, stratosphere, and ionosphere on the boresight error. Tropospheric and stratospheric effects are calculated assuming that the ionosphere is a vacuum. Also, ionospheric effects are computed assuming that the troposphere and stratosphere are vacuum. The boresight error in the troposphere and
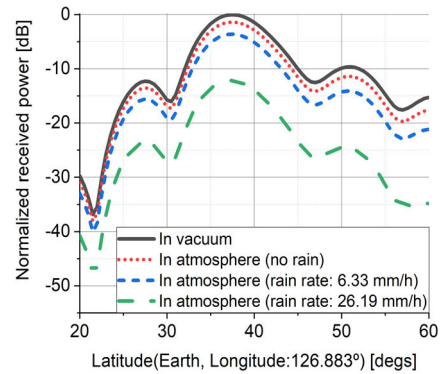

FIGURE 13. Normalized received power on downlink (transmit location: GEO, receiving location: 128.2°E, South Korea, Aug. 14, 2019).

TABLE 3. The calculated information (satellite: GEO, 128.2°E).

Environments (rain rate)	Maximum point (received power)	Boresight error [degs]	Distance error [m]	Power difference [dB]
(a) In vacuum	37.537° N 126.884° E	-	-	-
(b) In atmosphere (0 mm/h)	37.468° N 126.885° E	0.0085	7673	1.3801
(c) In atmosphere (6.33 mm/h)	37.425° N 126.887° E	0.0138	12457	3.6403
(d) In atmosphere (26.19 mm/h)	37.266° N 126.894° E	0.0336	30147	12.1621

stratosphere is almost constant, while the boresight error in the ionosphere decreases as the frequency increases.

Fig. 13 shows the normalized received power of an offset parabolic reflector antenna relative to the latitude of the earth at the GEO satellite with an east longitude of 128.2 degrees when the direction of antenna is towards the receiving point with latitude of 37.546 degrees and longitude 126.883 degrees. It is assumed that the rain distribution is uniform under the rain height. When rainfall rates are 0 mm/h, 6.33 mm/h, and 26.19 mm/h, the main beam moves 0.059 degrees (or 6561 m), 0.1 degrees (or 11119 m), and 0.258 degrees (or 28688 m), respectively, compared with the case of vacuum. Attenuation of the main beam is 1.38 dB, 3.59 dB, and 12.16 dB, respectively, when the rainfall rate is 0, 6.33, and 26.19 mm/h.

Fig. 14 illustrates the normalized received power by latitude and longitude from the GEO satellite to the Korean Peninsula. The normalized received power is the ratio of the received power to the maximum received power of the vacuum case at Seoul, Korea. As the observation point moves away from Seoul, the received power decreases. The boresight error and attenuation in each case are given in Table 3.

The maximum point of the received power in each case depends on the atmospheric environments. As the rain rate increases, the maximum points move southeast. The distance error is calculated using the boresight error and radius of the earth. The power difference is the subtraction of the maximum received power in vacuum and maximum received power in each environment, and is regarded as the
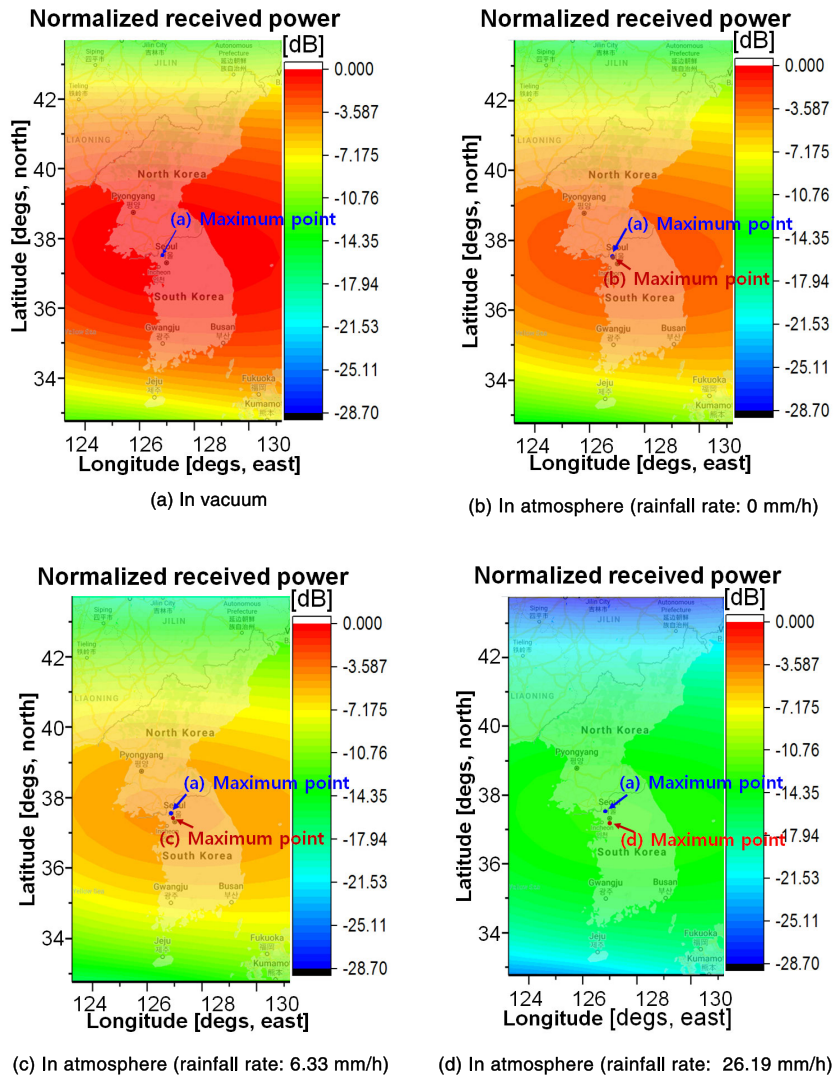
(a) In vacuum

(b) In atmosphere (rainfall rate: 0 mm/h)

(c) In atmosphere (rainfall rate: 6.33 mm/h)

(d) In atmosphere (rainfall rate: 26.19 mm/h)

FIGURE 14. Normalized received power on Korean Peninsula. (earth station: 37.546°N, 126.88°E, satellite: GEO, 128.2°E, Osan, Aug. 14, 2019).

atmospheric attenuation. As the rainfall rate increases, the atmospheric attenuation and boresight error increases.

III. CONCULSION

The method to calculate the propagation from GEO satellites to a ground station considering dispersive and inhomogeneous atmospheric environments with an actual satellite parabolic reflector antenna has been proposed. The proposed simulation method is based on high-frequency approximation including PO, 3-D ray tracing technique, and GO. An electromagnetic propagation from the actual GEO satellite parabolic reflector antenna was calculated by using PO, and reflections and refractions at the boundaries of the stratified refractive index model for the atmosphere were computed by ray tracing technique and GO. Our method showed good agreements with the results with the prediction method of rain attenuation given in ITU-R P.618-13 and the unified model. We have also discussed how the inhomogeneity and dispersion of the atmosphere affect the wave propagation in terms

of attenuation and boresight error from the GEO satellites to the ground station at Seoul, Korea. Our method is useful for accurately estimating the electromagnetic wave propagation on GEO satellite links for navigation, communications, broadcasting, and surveillance.

REFERENCES

[1] D. Roddy, "Radio wave propagation," in *Satellite Communications*, 4th ed. New York, NY, USA: McGraw-Hill, 2006, pp. 103–113.

[2] J. Miguel Garcia-Rubia, J. M. Riera, P. Garcia-del-Pino, and A. Benarroch, "Propagation in the ka band: Experimental characterization for satellite applications," *IEEE Antennas Propag. Mag.*, vol. 53, no. 2, pp. 65–76, Apr. 2011.

[3] P. M. Kalaivaanan, A. Sali, R. S. A. Raja Abdullah, S. Yaakob, M. Jit Singh, and A. M. Al-Saegh, "Evaluation of ka-band rain attenuation for satellite communication in tropical regions through a measurement of multiple antenna sizes," *IEEE Access*, vol. 8, pp. 18007–18018, Jan. 2020.

[4] *Propagation Data and Prediction Methods Required for the Design of Earth-Space Telecommunication Systems*, document Recommendation ITU-R 618-13, Dec. 2017.

[5] H. J. Liebe, "MPM an atmospheric millimeter-wave propagation model," *Int. J. Infr. Millim. Waves*, vol. 10, no. 6, pp. 631–650, Jun. 1989.

[6] H. J. Liebe, "Propagation modeling of moist air and suspended water/ice particles below 1000 GHz," in *Proc. 52nd Specialists' Meeting Electromagn. Wave Prop. Panel*, Palma de Mallorca, Spain, 1993, pp. 3-1–3-10.

[7] X. Liu, J. Yue, J. Xu, W. Yuan, J. M. Russell, and M. E. Hervig, "Five-day waves in polar stratosphere and mesosphere temperature and mesospheric ice water measured by SOFIE/AIM," *J. Geophys. Res., Atmos.*, vol. 120, no. 9, pp. 3872–3887, May 2015.

[8] R. G. Pinnick, J. M. Rosen, and D. J. Hofmann, "Stratospheric aerosol measurements III: Optical model calculations," *J. Atmos. Sci.*, vol. 33, no. 2, pp. 304–314, Feb. 1976.

[9] C. Jiang, "Ionosonde observations of daytime spread F at low latitudes," *J. Geophys. Res., Space Phys.*, vol. 121, no. 12, p. 12,093-12,103, Nov. 2016.

[10] T. Moffat-Griffin, C. J. Wright, A. C. Moss, J. C. King, S. R. Colwell, J. K. Hughes, and N. J. Mitchell, "The south georgia wave experiment (SG-WEX): Radiosonde observations of gravity waves in the lower stratosphere. Part I: Energy density, momentum flux and wave propagation direction," *Quart. J. Roy. Meteorol. Soc.*, vol. 143, no. 709, pp. 3279–3290, Oct. 2017.

[11] M. Grabner, P. Pechac, and P. Valtr, "Analysis of propagation of electromagnetic waves in atmospheric hydrometeors on low-elevation paths," *Radioengineering*, vol. 27, no. 1, pp. 29–33, Apr. 2018.

[12] J. M. G. Rubia, "Experimental assessment of slant path rain attenuation variability in the Ka band," *Int. J. Satell. Commun. Netw.*, vol. 34, no. 2, pp. 155–170, Mar./Apr. 2016.

[13] L. Luini, C. Riva, and L. Emiliani, "Attenuation induced by water vapor along Earth-space links: Selecting the most appropriate prediction method," *IEEE Trans. Antennas Propag.*, vol. 65, no. 7, pp. 3806–3808, Jul. 2017.

[14] L. Luini and C. G. Riva, "A simplified model to predict oxygen attenuation on Earth-space links," *IEEE Trans. Antennas Propag.*, vol. 65, no. 12, pp. 7217–7223, Dec. 2017.

[15] A. Battaglia, K. Mroz, D. Watters, and F. Ardhuin, "GPM-derived climatology of attenuation due to clouds and precipitation at ka-band," *IEEE Trans. Geosci. Remote Sens.*, vol. 58, no. 3, pp. 1812–1820, Mar. 2020.

[16] *Attenuation by Atmospheric Gases and Related Effects*, document Recommendation ITU-R 676-12, Aug. 2019.

[17] T. Halder, A. Adhikari, and A. Maitra, "Rain attenuation studies from radiometric and rain DSD measurements at two tropical locations," *J. Atmos. Solar-Terrestrial Phys.*, vol. 170, pp. 11–20, May 2018.

[18] H. Chung, "Accurate FDTD dispersive modeling for concrete materials," *ETRI J.*, vol. 35, no. 5, pp. 915–918, Oct. 2013.

[19] H. Choi, J.-W. Baek, and K.-Y. Jung, "Comprehensive study on numerical aspects of modified lorentz model-based dispersive FDTD formulations," *IEEE Trans. Antennas Propag.*, vol. 67, no. 12, pp. 7643–7648, Dec. 2019.

[20] P. Zhang, L. Bai, Z. Wu, and L. Guo, "Applying the parabolic equation to tropospheric groundwave propagation: A review of recent achievements and significant milestones.," *IEEE Antennas Propag. Mag.*, vol. 58, no. 3, pp. 31–44, Jun. 2016.

[21] L. S. Mello and M. S. Pontes, "Unified method for the prediction of rain attenuation in satellite and terrestrial links," *J. Microw., Optoelectron. Electromagn. Appl.*, vol. 11, no. 1, pp. 01–14, Jun. 2012.

[22] C. Kim and Y. B. Park, "Prediction of electromagnetic wave propagation in space environments based on geometrical optics," *J. Electromagn. Eng. Sci.*, vol. 17, no. 3, pp. 165–167, Jul. 2017.

[23] J.-S. Choi, Y.-D. Lee, and S. P. Lee, "CATR test for ka band multi-beam antenna," in *Proc. 26th Int. Commun. Satell. Syst. Conf. (ICSSC)*, Jun. 2008, pp. 1–5.

[24] M. P. Richardson, "Physical optics based methods for scattering analysis," Ph.D. dissertation, Dept. Elect. Electron. Eng., Stellenbosch Univ., Stellenbosch, South Africa, 2018.

[25] C. A. Balanis, *Antenna Theory: Analysis and Design*, 4th ed. Hoboken, NJ, USA: Wiley, 2016.

[26] K. G. Budden, *Radio Waves in the Ionosphere, Radio Waves in the Ionosphere*. Cambridge, U.K.: Cambridge Univ. Press, 2009.

[27] B. Zolesi, and L. R. Cander, *Ionospheric Prediction and Forecasting*. Berlin, Germany: Springer, 2014.

[28] *Didbase*. Accessed: Aug. 8, 2019. [Online]. Available: https://ulcar.uml.edu/DIDBase

[29] *Ionospheric Propagation Data and Prediction Methods Required for the Design of Satellite Services and Systems*, document Recommendation ITU-R-531, 2019.

[30] *Real time GPS Scintillation Monitor*. Accessed: Jul. 3, 2019. [Online]. Available: https://spaceweather.rra.go.kr/observation/ground/sciserial

[31] *Atmospheric Soundings*. Accessed: Jul. 3, 2019. [Online]. Available: http://weather.uwyo.edu/upperair/sounding.html

[32] C. A. Balanis, *Advanced Engineering Electromagnetics*, 2nd ed. Hoboken, NJ, USA: Wiley, 2012.

[33] S. Shrestha and D.-Y. Choi, "Study of rain attenuation in ka band for satellite communication in South Korea," *J. Atmos. Solar-Terrestrial Phys.*, vol. 148, pp. 53–63, Oct. 2016.

[34] J. S. Mandeep and S. I. S. Hassan, "60- to 1-Min rainfall-rate conversion: Comparison of existing prediction methods with data obtained in the southeast Asia region," *J. Appl. Meteorol. Climatol.*, vol. 47, no. 3, pp. 925–930, Mar. 2008.

[35] *Specific Attenuation Model for Rain for Use in Prediction Methods*, document Recommendation ITU-R-838, 2005.

[36] *Characteristics of Precipitation for Propagation Modeling*, document Recommendation ITU-R-837, 2017.

[37] *Rain Height Model for Prediction Methods*, document Recommendation ITU-R-839, 2013.

CHANGSEONG KIM (Student Member, IEEE) received the B.S. degree from the Department of Electrical and Computer Engineering, Ajou University, Suwon, South Korea, in 2015, where he is currently pursuing the integrated M.S./Ph.D. degree. His research interests include electromagnetic wave propagation and metasurface antenna.

JUN HEO (Student Member, IEEE) received the B.S. degree from the Department of Electrical and Computer Engineering, Ajou University, Suwon, South Korea, in 2018, where he is currently pursuing the M.S./Ph.D. degree. His research interests include wireless power transfer and electromagnetic wave propagation.

KYUNG-YOUNG JUNG (Senior Member, IEEE) received the B.S. and M.S. degrees in electrical engineering from Hanyang University, Seoul, South Korea, in 1996 and 1998, respectively, and the Ph.D. degree in electrical and computer engineering from The Ohio State University, Columbus, OH, USA, in 2008. From 2008 to 2009, he was a Postdoctoral Researcher with The Ohio State University. From 2009 to 2010, he was an Assistant Professor with the Department of Electrical and Computer Engineering, Ajou University, Suwon, South Korea. Since 2011, he has been with Hanyang University, where he is currently an Associate Professor with the Department of Electronic Engineering. His current research interests include computational electromagnetics, bio-electromagnetics, and nano-electromagnetics. He was a recipient of the Graduate Study Abroad Scholarship from the National Research Foundation of Korea, the Presidential Fellowship from The Ohio State University, the Best Teacher Award from Hanyang University, and the Outstanding Research Award from the Korean Institute of Electromagnetic Engineering Society.

HOSUNG CHOO (Senior Member, IEEE) received the B.S. degree in radio science and engineering from Hanyang University, Seoul, South Korea, in 1998, and the M.S. and Ph.D. degrees in electrical and computer engineering from The University of Texas at Austin, in 2000 and 2003, respectively. He joined the School of Electronic and Electrical Engineering, Hongik University, Seoul, in 2003, where he is currently a Professor. His research interests include electrically small antennas for wireless communications, reader and tag antennas for RFID, on-glass and conformal antennas for vehicles and aircraft, and array antennas for GPS applications.

YONG BAE PARK (Senior Member, IEEE) received the B.S., M.S., and Ph.D. degrees in electrical engineering from the Korea Advanced Institute of Science and Technology, South Korea, in 1998, 2000, and 2003, respectively. From 2003 to 2006, he was with the Korea Telecom Laboratory, Seoul, South Korea. He joined the School of Electrical and Computer Engineering, Ajou University, South Korea, in 2006, where he is currently a Professor. His research interests include electromagnetic field analysis, high-frequency methods, metamaterial antennas, radomes, and stealth technology.

• • •